No-search algorithm for direction of arrival estimation

T. Engin Tuncer[1] and M. Tankut Özgen[2]

Received 20 February 2009; revised 9 May 2009; accepted 15 May 2009; published 30 September 2009.

[1] Direction of arrival estimation (DOA) is an important problem in ionospheric research and electromagnetics as well as many other fields. When superresolution techniques are used, a computationally expensive search should be performed in general. In this paper, a no-search algorithm is presented. The idea is to separate the source signals in the time-frequency plane by using the Short-Time Fourier Transform. The direction vector for each source is found by coherent summation over the instantaneous frequency (IF) tracks of the individual sources which are found automatically by employing morphological image processing. Both overlapping and nonoverlapping source IF tracks can be processed and identified by the proposed approach. The CLEAN algorithm is adopted in order to isolate the IF tracks of the overlapping sources with different powers. The proposed method is very effective in finding the IF tracks and can be applied for signals with arbitrary IF characteristics. While the proposed method can be applied to any sensor geometry, planar uniform circular arrays (UCA) bring additional advantages. Different properties of the UCA are presented, and it is shown that the DOA angles can be found as the mean-square error optimum solution of a linear matrix equation. Several simulations are done, and it is shown that the proposed approach performs significantly better than the conventional methods.

Citation: Tuncer, T. E., and M. T. Özgen (2009), No-search algorithm for direction of arrival estimation, *Radio Sci.*, *44*, RS5007, doi:10.1029/2009RS004164.

1. Introduction

[2] The estimation of direction of arrival (DOA) is an important problem in radar, sonar, seismology and geophysics. DOA estimation is used to measure the drift in ionospheric plasma [*Parkinson et al.*, 1997] and to separate the source signals [*Hirari and Hayakawa*, 1999]. Superresolution DOA estimation methods are popular due to their close to optimum use of the sensor signals and high resolution [*Tuncer et al.*, 2007]. These methods return estimates whose ultimate performance is compared with the Cramer-Rao Bound (CRB) [*Stoica and Nehorai*, 1990; *Weiss and Friedlander*, 1993], which is seen as a benchmark for unbiased estimators. In the work of *Belouchrani and Amin* [1999], a new approach for DOA estimation of narrowband signals by using time-frequency distributions is proposed. This work opened up new possibilities and opportunities. It is followed by the works on wideband DOA estimation [*Gershman and Amin*, 2000] and chirp beamforming for nonstationary signals [*Gershman et al.*, 2001]. In the work of *Gershman et al.* [2001], it is shown that results better than the conventional (or benchmark) CRB can be achieved if the signal model is employed over a 3-*D* search in parameter space. Furthermore a CRB for the new problem setting based on the polynomial phase signal (PPS) model, is presented.

[3] In this paper, a no-search algorithm (NSA) is presented for DOA estimation. NSA does not require a search which is an important advantage especially for array geometries different than uniform linear array (ULA). We call this algorithm as NSA instead of a fast algorithm since the computational complexity depends on the number of snapshots. It turns out that the complexity of the NSA for the nonoverlapping sources is significantly less than the exhaustive search algorithms when the number of snapshots is sufficiently low (ex. $N < 400$).

[1]Electrical and Electronics Engineering Department, Middle East Technical University, Ankara, Turkey.
[2]Electrical and Electronics Engineering Department, Anadolu University, Eskişehir, Turkey.

0048-6604/09/2009RS004164

[4] The basic idea for the proposed approach is to isolate the source signals in the time-frequency plane. In the literature, the Wigner-Ville distribution (WVD) is usually employed for this purpose [*Belouchrani and Amin*, 1999; *Gershman and Amin*, 2000; *Heidenreich et al.*, 2007]. WVD has high resolution but it has cross terms that spill onto auto terms which generate a large error term in DOA estimation together with noise. Cross terms can be twice as large as the auto terms depending on the source signals. The effect of cross terms as well as noise can be reduced by spatial averaging [*Zhang and Amin*, 2000]. Unfortunately, spatial averaging should be applied over a large number of time-frequency points in order to have a meaningful decrease of the cross terms. Furthermore a smoothing window should be selected and pseudo-WVD should be used to decrease the effects of cross terms without degrading the auto terms significantly [*Stankovic et al.*, 1997; *Barkat et al.*, 1999]. On the other hand, STFT offers a computationally efficient alternative which is free of cross terms. The main disadvantage of STFT is its low resolution compared to the WVD. Auto terms in STFT distribution are not free of "cross-talk" effects due to finite sidelobe attenuation of the analysis window. The "cross-talk" effects are usually observed at high SNR. In this work, we use STFT and morphological image processing [*Högbom*, 1974] for DOA estimation. STFT is used for DOA estimation by *Zhou et al.* [2004]. In the work of *Aissa-El-Bey et al.* [2007], STFT is employed for source separation in case of nondisjoint or overlapping IF tracks of source signals by using a subspace projection operation. Each source is assumed to have a region in the time-frequency plane where this source exists alone. One of the main advantages of the proposed approach compared to the previous works is that morphological image processing together with the CLEAN algorithm results in a simple and effective method to isolate the IF tracks of arbitrary source signals. On the other hand, the proposed method may not be suitable for phase modulated signals which do not have continuous IF tracks or when there is multipath. CLEAN algorithm is well known in astronomy [*Clark*, 1980; *Schwarz*, 1978] and radar [*Abramovich*, 1978; *Tsao and Steinberg*, 1988; *Deng*, 2004], especially to reduce the sidelobe artifacts. There are different versions of CLEAN algorithm in the literature. The main idea for these algorithms is the same, namely, to remove the strongest signals from the observed data successively. Some of these algorithms operate over the observed signals [*Tsao and Steinberg*, 1988], and other versions operate over the covariance matrix or the spatial spectrum [*Stoica and Moses*, 2005]. The performance and behavior of these algorithms are different in general. Recently, it has been shown that the CLEAN algorithm is very effective in isolating the spatial spectrum of multiple signals [*Tuncer and Friedlander*, 2009]. In this paper, we use the sample-based CLEAN algorithm [*Tuncer and Friedlander*, 2009; *Tsao and Steinberg*, 1988] for isolating the IF track of sources.

[5] The contributions in this paper can be summarized as follows. Morphological image processing is used in STFT distributions in order to isolate the source IF tracks. CLEAN algorithm is adopted for this purpose which also allows the estimation of sources when the difference between signal powers is large. The proposed approach works effectively for overlapping sources. Multisource DOA problem is converted into a single-source one. A no-search algorithm is presented for DOA estimation. The algorithm is based on the indirect solution of a linear matrix equation in MSE optimum sense for the UCA. The proposed approach is general in the sense that any signal with an arbitrary continuous IF curve in time-frequency plane can be processed.

2. Model And Time-Frequency Representation

[6] We assume that there are n narrowband plane waves impinging on a sensor array with M elements. The narrowband assumption in this paper is the same as in the works of *Belouchrani and Amin* [1999] and *Zhang and Amin* [2000]. Therefore the time that the wave propagates across the array, τ, and the signal bandwidth, B, satisfy: $B\tau \ll 1$. The sensor output vector $\mathbf{x}(t)$ is given as,

$$\mathbf{x}(t) = \mathbf{A}(\theta)\mathbf{s}(t) + \mathbf{n}(t) \tag{1}$$

where $\mathbf{n}(t)$ is white Gaussian noise, $\mathbf{A}(\theta) = [\mathbf{a}(\theta_1) \ldots \mathbf{a}(\theta_n)]$ is the $M \times n$ steering matrix for the source DOA angles θ_i. $\mathbf{s}(t)$ is the $n \times 1$ source vector at time t and there are N snapshots for $t = 1,\ldots N$. In our case, there is no limitation on the type of signal characteristics as long as it has at least a segment of a continuous IF track in the time-frequency plane which is not corrupted by other sources. Nevertheless, we consider constant amplitude frequency modulated (FM) signals like $s_k(t) = \alpha_k e^{j\varphi_k}(t)$ for $k = 1,\ldots, n$ which are used in ionosphere sounding [*Davydenko et al.*, 2008]. The instantaneous frequency for the source signal is to be found automatically by using the STFT distribution of the signals. STFT is a linear time-frequency distribution and it is defined as,

$$\mathbf{S}_{\mathbf{x}}(t,f) = \sum_{\tau=-\infty}^{\infty} \mathbf{x}(\tau) w(\tau - t) e^{-j2\pi f \tau} \tag{2}$$

where $w(t)$ is the analysis window. If the above expression is combined with (1), we have,

$$\mathbf{S}_{\mathbf{x}}(t,f) = \mathbf{A}(\theta)\mathbf{S}_{\mathbf{s}}(t,f) + \mathbf{S}_{\mathbf{n}}(t,f) \tag{3}$$

[7] If the sources are disjoint in time-frequency plane, the above expression can be written for a single source as,

$$\mathbf{S_x}(t_k,f_k) = \mathbf{a}(\theta_i)S_{\mathbf{s}_i}(t_k,f_k) + \mathbf{S_n}(t_k,f_k) \quad \forall(t_k,f_k) \in \Gamma_i \tag{4}$$

where $i = 1,\ldots, n$, Γ_i is the set of time-frequency points (or IF track) of the i^{th} source and $S_{\mathbf{s}_i}(t_k, f_k)$ is the STFT of the i^{th} source signal at (t_k, f_k). Note that even though the sources overlap, we assume that it is possible to find regions in the time-frequency plane where only a single source exists. Therefore equation (4) is valid for those regions. The "cross-talk" effect for multiple sources due to finite sidelobe of the analysis window is assumed to be low and ignored in (4).

3. No-Search Algorithm

[8] NSA is based on equation (4). The importance of this equation is that a multisource problem is converted to a single-source one. This generates several advantages. More specifically, we can find the DOA angles directly without a search process. In the work of *Weiss and Friedlander* [1996], a DOA estimation algorithm without a search is proposed. It is assumed that the sensor gain patterns are identical and steering matrix $\mathbf{A}(\theta)$ is found for the multisource case by using an iterative approach. Nominal array manifold is assumed to be known approximately while a unique solution cannot be guaranteed in general [*Weiss and Friedlander*, 1996]. In our case, we convert the multisource problem to a single-source one and solve only a single linear matrix equation to find the DOA angle.

[9] Direction vector for the i^{th} source, $\mathbf{a}(\theta_i)$, can be found from (4) directly. In fact, in (4), we have a scaled and noise corrupted direction vector. If we have spatial averaging as in the work of *Zhang and Amin* [2000], we obtain a significantly better result. As the number of time-frequency points for spatial averaging increases, the performance increases. Therefore, direction vector estimate can be found as,

$$\hat{\mathbf{a}}(\theta_i) = \frac{1}{K}\sum_{k\in\Gamma_i}\frac{\mathbf{S_x}(t_k,f_k)}{S_{\mathbf{x}_k}(1)} \tag{5}$$

where K is the number of time-frequency points in Γ_i and $S_{x_k}(1)$ is the first element of the vector $\mathbf{S_x}(t_k, f_k)$. The normalization in the above expression removes the scale ambiguity and allows coherent summation which in turn improves the performance. Note that (5) can be used in a chirp beamformer [*Gershman et al.*, 2001] which does a 3-*D* search over the parameters and therefore uses the advantage of the signal model. In our case, we prefer a computationally simpler approach with no-search and we will not assume any signal model to have a more general treatment of the problem. On the other hand, we will also consider the STFT-MUSIC algorithm with 1-*D* search in order to have an idea about the application of conventional techniques in comparison to the STFT-NSA method.

[10] The next step is to find the DOA azimuth angle θ_i given $\hat{\mathbf{a}}(\theta_i)$. We will follow a similar approach as in the work of *Weiss and Friedlander* [1996], but an indirect and better solution is found for the linear matrix equation specifically for the UCA. Let the phase vector of the steering vector $\mathbf{a}(\theta_i)$ in (1) be $\mathbf{\Phi}_i = \arg\{\mathbf{a}(\theta_i)\}$. The elements of this phase vector can be written as,

$$\phi_i(m) = \frac{2\pi}{\lambda}\left[d_{x_m}\cos(\theta_i)\sin(\gamma_i) + d_{y_m}\sin(\theta_i)\sin(\gamma_i) + d_{z_m}\cos(\gamma_i)\right] \quad m = 1,\ldots,M \tag{6}$$

where d_{x_m}, d_{y_m}, and d_{z_m} are the Cartesian coordinates for the the m^{th} sensor. Wavelength is $\lambda = c/f$ and c is the speed of wave, f is the frequency. Since $\phi_i(m)$ is ambiguous by 2π, phase unwrapping must be applied as in the work of *Weiss and Friedlander* [1996]. If we assume that there are $M = 8$ sensors on a circular array with intersensor distance $d_s = \lambda/2$ and $\gamma_i = \pi/2$ for simplicity, then $|\phi_i(m)| \leq 1.3\pi$. Therefore only $\pm 2\pi$ phase jumps occur. A logic statement based on the elements of $\phi_i(m)$ can be used to detect the phase jumps and the correction by $\pm 2\pi$ can be done. It turns out that only a few phase jumps occur and they can be easily corrected. In our case, we used only four logic statements in order to have the phase unwrapping.

[11] Let $\mathbf{D}$ be the $M \times 3$ matrix for sensor positions,

$$\mathbf{D} = \begin{bmatrix} d_{x_1} & d_{y_1} & d_{z_1} \\ d_{x_2} & d_{y_2} & d_{z_2} \\ \vdots & \vdots & \vdots \\ d_{x_M} & d_{y_M} & d_{z_M} \end{bmatrix} \tag{7}$$

and $\mathbf{\Psi}_i = [\cos(\theta_i)\ \sin(\gamma_i)\ \sin(\theta_i)\ \sin(\gamma_i)\ \cos(\gamma_i)]^T$ is the vector for azimuth, θ_i, and elevation angle γ_i. When the array model in (1) is considered, we obtain,

$$\frac{2\pi}{\lambda}\mathbf{D}\mathbf{\Psi}_i = \mathbf{\Phi}_i \quad i = 1,2,\ldots,n \tag{8}$$

As it is pointed before, normalization and coherent summation as in (5) improves the estimation performance. Let $\mathbf{D_1} = \mathbf{D} - \mathbf{1}\,[d_{x_1}\ d_{y_1}\ d_{z_1}]$ where $\mathbf{1} = [1\ \ldots\ 1]^T$ is a $M \times 1$ vector and $\mathbf{\Phi}_i = [\phi_i(1)\ \phi_i(2)\ \ldots\ \phi_i(M)]^T$. Assuming that $\overline{\mathbf{\Phi}}_i = \mathbf{\Phi}_i - \phi_i(1)\mathbf{1}$ is the phase vector due

to normalization in (5), we can write the following linear equation,

$$\frac{2\pi}{\lambda}\mathbf{D}_1\boldsymbol{\Psi}_i = \overline{\boldsymbol{\Phi}}_i \quad i = 1, 2, \ldots, n \tag{9}$$

It turns out that it is possible to find two different ways for determining $\boldsymbol{\Psi}_i$. In the first case, we can take into account the normalization in (5) and obtain (9). This algorithm is no-search algorithm with direct computation and denoted as NSA-D. The solution for the NSA-D can be found as,

$$\hat{\boldsymbol{\Psi}}_i = \frac{\lambda}{2\pi}\left(\mathbf{D}_1^H\mathbf{D}_1\right)^{-1}\mathbf{D}_1^H\overline{\boldsymbol{\Phi}}_i \tag{10}$$

[12] The second algorithm is the original no-search algorithm, namely NSA. NSA algorithm can be seen as an indirect approach and solves the following equation,

$$\frac{2\pi}{\lambda}\mathbf{D}\boldsymbol{\Psi}_i = \overline{\boldsymbol{\Phi}}_i \quad i = 1, 2, \ldots, n \tag{11}$$

by Moore-Penrose pseudoinverse as in the NSA-D case,

$$\tilde{\boldsymbol{\Psi}}_i = \frac{\lambda}{2\pi}\left(\mathbf{D}^H\mathbf{D}\right)^{-1}\mathbf{D}^H\overline{\boldsymbol{\Phi}}_i \tag{12}$$

In the following part of this paper, it is shown that the solution for (11) corresponds to the MSE optimum one under the assumption that the geometric center of the circular array is the origin of the coordinate system. In this case, the measured phase vector, $\boldsymbol{\Phi}_i$, which is relative to the coordinate origin, can be replaced with the differential phase vector, $\overline{\boldsymbol{\Phi}}_i$, which is with respect to the first (or any other) sensor. Since the columns of D are orthogonal to the vector **1**, the least squares solution for (11) is invariant to the subtraction of any constant phase vector. In fact, if we multiply (9) from left by $\mathbf{D}^H$, we obtain $(2\pi/\lambda)\mathbf{D}^H\mathbf{D}\boldsymbol{\Psi}_i = \mathbf{D}^H\overline{\boldsymbol{\Phi}}_i$ which in turn gives (12).

[13] NSA and NSA-D algorithms return exactly the same solution for the error-free case, whereas their performances differ significantly when there is error in phase terms. It can be shown that the mean-square error of $\psi_i(1)$ for the NSA solution is $(\lambda/2\pi)^2 2\sigma_e^2/(r^2M)$ and the ratio of the mean-square errors of the NSA and NSA-D algorithms for $\psi_i(1)$ is

$$\frac{MSE_{NSA}}{MSE_{NSA-D}} = \frac{9}{2M+3} \tag{13}$$

[14] The error for $\psi_i(2)$ is same for both algorithms. Therefore NSA algorithm performs better than the NSA-D for $M > 3$. In the following parts of this paper, we will only consider the NSA algorithm and the equations in (11) and (12).

[15] Note that $\boldsymbol{\Psi}_i$ has unit norm and this can be added as a constraint in equation (11). Since $\mathbf{D}^H\mathbf{D}$ is a diagonal matrix, the solution in (12) and the solution for the constrained equation are same up to a scale factor. It turns out that the scale factor does not change the estimated azimuth angle.

[16] Once $\boldsymbol{\Psi}_i$ is found from (12), DOA azimuth angle θ_i can be obtained as,

$$\theta_i = \tan^{-1}\left(\frac{\psi_i(2)}{\psi_i(1)}\right) \tag{14}$$

[17] Elevation angle, γ_i, can be computed in a simple manner as,

$$\gamma_i = \sin^{-1}\left(\sqrt{\psi_i(1)^2 + \psi_i(2)^2}\right) \tag{15}$$

[18] The proposed approach for DOA estimation can be applied for arbitrary array geometries but the advantages of the method are mainly seen in circular arrays. Circular arrays have certain properties which will be outlined in Lemma 1. The solution for the equation in (11) can be found in MSE optimum manner due to these properties. In this respect, we will mainly concentrate on the uniform circular arrays. In the following lemma, the properties of UCA are presented.

Lemma 1

Let $\mathbf{d}_i = [d_{x_i}\ d_{y_i}\ d_{z_i}]$ be the vector of Cartesian coordinates of the i^{th} sensor on a planar circular array with equal interelement distances, d_s. $d_{z_i} = z_0 = 0$ is selected $\forall i$ and the radius of the circular array is $r = \frac{d_s/2}{\sin(\pi/M)}$. **D** is a matrix of sensor coordinates as in (7) and

$$d_{x_j} = r\cos\left(\frac{2\pi}{M}(j-1)\right) \quad j = 1, 2, \ldots, M \tag{16}$$

$$d_{y_j} = r\sin\left(\frac{2\pi}{M}(j-1)\right) \tag{17}$$

$$d_{z_j} = z_0 = 0 \tag{18}$$

Then the following equations are true for $M \geq 3$:

(a)
$$\sum_{j=1}^{M} d_{x_j} = 0 \tag{19}$$

(b)
$$\sum_{j=1}^{M} d_{y_j} = 0 \tag{20}$$

(c) $$\sum_{j=1}^{M} d_{x_j} d_{y_j} = 0 \tag{21}$$

(d) $$\sum_{j=2}^{M} \left(d_{x_j} - d_{x_1}\right)\left(d_{y_j} - d_{y_1}\right) = 0 \tag{22}$$

(e) $$\sum_{j=1}^{M} d_{x_j}^2 = c_1 = r^2 M/2 \tag{23}$$

(f) $$\sum_{j=1}^{M} d_{y_j}^2 = c_1 = r^2 M/2 \tag{24}$$

(g) $$\mathbf{D^H D} = diag(c_1, c_1, 0) \tag{25}$$

Proof of this lemma is given in Appendix A.

Note that the coordinate axis can always be chosen to satisfy the relations in (16)–(18). Also only the first two elements of $\mathbf{\Psi}_i$ and first two columns of $\mathbf{D}$ in (11) are required in order to find both the azimuth and elevation angles as in (14) and (15), respectively. In this case, the constraint on $\mathbf{\Psi}_i$ is converted to an inequality. Fortunately, this inequality constraint does not affect the solution due to Lemma 1.g.

In the following theorem, it is shown that the MSE optimum Wiener solution for the equation (11) and the solution in (12) are same up to a scale factor.

Theorem 1

Let M be the number of sensors in a circular array with radius r and $n < M$. Assume that the differential phase has an error $\mathbf{e}$ and the MSE optimum Wiener solution in equation (11) is obtained as $\breve{\mathbf{\Psi}}_i = \lambda/(2\pi)\mathbf{G}(\overline{\mathbf{\Phi}}_i + \mathbf{e})$ where $\mathbf{G} = \sigma_\psi^2 \mathbf{D}^H(\sigma_\psi^2 \mathbf{D}\mathbf{D}^H + \sigma_e^2 \mathbf{I})^{-1}$. Similarly, $\overline{\mathbf{G}} = (\mathbf{D}^H\mathbf{D})^{-1}\mathbf{D}^H$ is used for the NSA algorithm as in (12). The covariance matrices are assumed as $\mathbf{R}_\psi = \sigma_\psi^2 \mathbf{I}$ and $\mathbf{R}_e = \sigma_e^2 \mathbf{I}$. $\mathbf{\Psi}$ and $\mathbf{e}$ are independent. Then the following relation between the Wiener and pseudo-inverse expressions is true,

$$\mathbf{G} = \frac{\sigma_\psi^2 c_1}{\sigma_\psi^2 c_1 + \sigma_e^2}\overline{\mathbf{G}} \tag{26}$$

Proof of this theorem is given in Appendix A.

The a–b items in Lemma 1 can be used to show that the columns of $\mathbf{D}$ are orthogonal to the vector $\mathbf{1}$. The c–g items in Lemma 1 and Theorem 1 show that the unit norm constraint for $\mathbf{\Psi}_i$ for the solution of (11) is irrelevant. Also the requirement for choosing the array geometric center as the origin of the coordinate axis is satisfied with Lemma 1.

4. Automatic IF Track Extraction

[19] In this paper, we consider the automatic IF track extraction by using morphological image processing techniques. This nonparametric approach allows us to deal with any kind of source IF characteristics. Most of the previous work considers the polynomial phase signals which are only a limited subset of the possible source characteristics. In this respect, we have a more general framework for the IF track extraction. The price paid for this is the relative increase in computational complexity for the overlapping sources and the performance loss especially for the polynomial phase signals. However further improvement of the performance is possible if the IF track parameters are estimated and a limited search is conducted in the parameter space.

[20] We present two different approaches for the automatic IF track extraction. The first approach is for the nonoverlapping (or disjoint) sources. While this case is seldom observed (except the single source case), it is important for the quantification of the performance of the proposed approach. The detection of this case in a general scenario is outside the scope of this paper and we will mainly focus on the performance of the proposed method in this idealistic case. A more general approach is the IF track extraction for the overlapping (or non-disjoint) sources. This approach is computationally more intense than the previous one. In return, sources can be more effectively handled. It is assumed that the sources are "well separated" as in the work of *Gershman et al.* [2001] since source DOA is used to associate the IF segments. We have adopted the CLEAN algorithm [*Schwarz*, 1978; *Högbom*, 1974] in order to isolate the IF tracks of each source effectively [*Tuncer and Friedlander*, 2009].

[21] In the works of *Heidenreich et al.* [2007] and *Borda et al.* [2005], morphological image processing is used to obtain the IF segments of the source signals. In the work of *Heidenreich et al.* [2007], source IF segments are assumed to be overlapping and WVD is employed. A smoothing window is used to reduce the cross terms which generate false IF segments. In this paper, we employ STFT which does not have cross terms. However the STFT distribution is not disjoint for each source and each STFT point contains contributions from other sources due to finite sidelobe attenuation of the analysis window, nonstationarity of the source signals, etc. Note that this is not as disturbing as the cross terms in WVD where the magnitude of the cross terms can be twice as large as the source components.

[22] The morphological image processing for the proposed approach is simple and can be realized essentially with three MATLAB commands. *bwmorph* with the "thin" and "clean" terms is used for thinning the binary image and cleaning the unconnected pixels. *bwmorph* command applies a specific morphological operation to the binary image. When the "thin" argument is used, pixels are removed to obtain a minimally connected trace. When the "clean" argument is used, isolated pixels are removed. bwlabel is used to label each IF segment and *find* is used to obtain the x and y coordinates of the nonzero pixels in the binary image. A detailed discussion of each of these morphological functions can be found in the work of *Dougherty and Lotufo* [2003]. In the following part, we present the automatic IF track extraction and DOA estimation method for nonoverlapping and overlapping sources separately.

4.1. Nonoverlapping Sources

[23] In this case, it is assumed that the source IF tracks do not overlap and the performance of the proposed NSA algorithm is considered. Once we have the STFT distribution for the signal, $\mathbf{S}_{\mathbf{x}_i}(t, f)$, in one of the sensor elements, we obtain a binary image composed of lines of one pixel thickness. In order to have such an image, a threshold is applied on the STFT magnitude. While the selection of this threshold is important, proposed approach is robust to the value of the threshold. This threshold is set to be half of the maximum value in the STFT magnitude distribution assuming that the source powers are not extremely different from each other. A smaller value of the threshold increases both the performance and computational complexity. Further discussion of the effect of the threshold selection is done for the overlapping sources in the following part. The IF skeleton is obtained by a thinning operation which also preserves the pixel connectivity. Short segments are deleted in order to keep only the source IF tracks which are assumed to be sufficiently long. In our case, we deleted the segments below 20 pixels. The elimination of spurious IF tracks due to noise and "cross talk" is more effectively done in the case of overlapping sources where CLEAN algorithm is employed.

[24] NSA for the nonoverlapping sources is simple, computationally efficient and effective. Assuming that the number of sources, n, is known, the algorithmic steps of the proposed algorithm are given below.

Step 1. Compute the STFT magnitude of one sensor signal and use a threshold to obtain a binary image.

Step 2. Obtain the IF skeleton by using a thinning operation while preserving the pixel connectivity.

Step 3. Remove short segments and isolated pixels.

Step 4. Label the longest n IF tracks for the sources. Obtain the set of time-frequency points belonging to each source, Γ_i, $i = 1, 2, \ldots, n$.

Step 5. Compute the STFT of remaining sensor signals. For each source angle θ_i, $i = 1, \ldots, n$,

[25] (i) Find the direction vector estimate from (5),

[26] (ii) Compute the DOA angle from (12), (14) and (15).

4.2. Overlapping Sources

[27] In this case, we assume that the source IF tracks overlap. Therefore isolation of the IF track of each source is an important problem in order to have a coherent summation as in equation (5). We adopted the CLEAN algorithm [*Högbom*, 1974] for source IF track isolation. CLEAN algorithm has been applied in astronomy [*Clark*, 1980], radar [*Deng*, 2004], beamforming [*Schwarz*, 1978], etc. The potential of CLEAN algorithm in DOA estimation has been mostly overlooked in the literature except in a limited number of sources [*Tsao and Steinberg*, 1988; *Tuncer and Friedlander*, 2009]. In the work of *Tsao and Steinberg* [1988], CLEAN algorithm is applied over the covariance matrix. In this paper, we use a sample-based approach as in the original CLEAN algorithm for source isolation.

[28] The proposed method, NSA, has the following algorithmic steps for the overlapping case:

Step 1. Compute the STFT magnitude of one sensor signal and use a threshold to obtain a binary image.

Step 2. Obtain the IF skeleton by using a thinning operation while preserving the pixel connectivity.

Step 3. Remove short segments and isolated pixels.

Step 4. Find the DOA for each STFT point corresponding to the indices of nonzero pixels obtained in step 3 by using equations (5), (12), and (14). Obtain the histogram of the DOA angles.

Step 5. Select the largest n peaks in the histogram. Take the initial DOA estimates, $\hat{\theta}_i$, for the sources as the angles corresponding to the peaks of the histogram.

Step 6. Construct the steering matrix $\hat{\mathbf{A}}$ and estimate the source signals from, $\hat{\mathbf{s}} = (\hat{\mathbf{A}}^H\hat{\mathbf{A}})^{-1}\hat{\mathbf{A}}^H\mathbf{x}$.

For each $\hat{\theta}_i$, $i = 1, \ldots, n$,

[29] (i) Construct the $M \times (n-1)$ steering matrix $\overline{\mathbf{A}}_i$. $\overline{\mathbf{A}}_i$ is obtained from $\hat{\mathbf{A}}$ by deleting the i^{th} column. Also obtain the source, $\overline{\mathbf{s}}_i$, from $\mathbf{s}$ by deleting the i^{th} row.

[30] (ii) Find the cleaned data for the i^{th} source as, $\mathbf{x}_i = \mathbf{x} - \overline{\mathbf{A}}_i\overline{\mathbf{s}}_i$

[31] (iii) Repeat the operations in steps 1–3 for the $\mathbf{x}_i$ and obtain the isolated IF track of the source i.

Step 7. Using the binary image of the isolated source tracks, find the crossing points and their indices by overlapping the IF tracks of the sources (through simple summation of the binary images).

Step 8. Use the indices of the isolated IF tracks obtained in step 6 to select the STFT points of the original signal $\mathbf{x}$. The selection should consider the distance of each STFT point from the crossing points found in step 7. If the distance from these crossing points

is greater than a certain value (in our case 20 pixels), then the STFT points for the source are used in equation (5). The true DOA for the source is computed by using (12), (14) and (15). Step 8 is repeated for each source.

[32] The CLEAN algorithm described in step 6 is very effective in obtaining the isolated IF tracks of the sources. One reason for this is its ability to remove signal components from the original signal **x** even when the initial DOA angles θ_i are not accurate. This comes with a price such that the STFT points which belong only to single source are also corrupted to some extent. In step 8, the STFT of the original signal is used to avoid such distortions and the result of the CLEAN algorithm is used only to obtain the isolated IF tracks of the individual sources. The selection of the STFT points based on their distances from the crossing points are due to the fact that NSA algorithm assumes that each STFT point is only due to a single source. At the crossing points and their neighborhoods, more than one source contribution violates this assumption. On the other hand, the contributions of the sources on each other's STFT points due to finite sidelobe attenuation of the analysis window are usually negligible at low SNR. Proposed method is robust to the selection of the threshold value in step 1. If the threshold is low, both the computational complexity and the performance in estimation of the initial DOA angles in step 5 increase. Furthermore low power source signals can be better detected in this case. Therefore the threshold value can be chosen based on the computational complexity versus the performance trade off. Note that in step 6.iii, a different and large threshold value (in our case 2/3 of the maximum value) is used since the STFT distribution has only one source and source points have the largest value. In simulations, we present an example in order to show the robustness and effectiveness of the proposed approach to deal with the different power sources.

5. Computational Complexity

[33] In this part, the computational complexity of the NSA algorithm for the nonoverlapping sources is discussed. The computational complexity of the algorithm for the overlapping sources is about ten times larger than the nonoverlapping case. There are three major contributors for the computational complexity of the proposed algorithm. The steps 1 through 6, where the IF track of the source signals are identified, requires 1/3 of the computation time. The steps 8 and 9, where the source DOA for each IF track is computed, take the 2/3 of the computation time. Half of the computation time in 8 and 9 comes from the STFT computation for the sensor outputs.

[34] The computational complexity of the NSA algorithm depends on the number of snapshots and it is one of the dominant terms. Computational complexity of NSA is approximately $O(M\frac{N^2}{2}log_2N + M^3)$. MUSIC algorithm requires an exhaustive search and the complexity of this search is the dominant term of the overall complexity of this algorithm. Assuming that A degrees of accuracy is desired, the computational complexity of MUSIC is approximately $O(M^3 + 2M\frac{360}{A})$. The computational complexity of NSA is significantly smaller than MUSIC even for large N (ex. $N < 400$) when $A = 0.001$ degrees and $M = 8$. It is possible to decrease the complexity of exhaustive search under certain assumptions. Specifically, if there are no two sources closer than $\Delta\theta$ degrees, a rough search with $\Delta\theta$ resolution and then a detailed search at the close neighborhood of the MUSIC peaks can be done. The complexity of such an approach is approximately $O(M^3 + 2M(\frac{360}{\Delta\theta} + \frac{n\Delta\theta}{A}))$. In such a case, NSA has less computational complexity when $N < 50$ if $\Delta\theta = 1$ degrees.

6. Simulations

[35] In this part, results for both nonoverlapping and overlapping sources are presented, respectively.

6.1. Nonoverlapping Sources

[36] The performance of the proposed approach is evaluated in a uniform circular array with $M = 8$ sensors. The radius of the circular array is set such that the distance between sensors is $\lambda/2$. The number of snapshots is $N = 256$ and the experiments reflect the result of 500 trials. The azimuth angles for the three source signals are 70, 90 and 105 degrees. The elevation angle is fixed at 90 degrees. Figure 1 shows the STFT distribution of the three sources when $SNR = 15$ dB. There are two chirp signals $s_2(t)$, $s_3(t)$ and a piecewise linear FM modulated real signal, $s_1(t)$. Phase term for the $s_2(t)$ and $s_3(t)$ signals, $s_k(t) = c_k e^{j\varphi_k}(t)$, is $\varphi_k(t) = w_{k,0}t + w_{k,1}t^2$. $s_1(t)$ is composed of symmetric chirp segments. The center frequencies are $w_{1,0} = \pi/5$, $w_{2,0} = 0.55\pi$ and $w_{3,0} = 0.7\pi$, respectively. The discrete-time chirp rates are $w_{1,1} = \pm 0.0028$, $w_{2,1} = -0.0014$ and $w_{3,1} = 0.0014$, respectively, for the source signals. Initial source amplitudes, c_k, are fixed and $c_1 = \sqrt{2}$, $c_2 = c_3 = 1$, respectively. When the morphological image processing process is applied, IF tracks as in Figure 2 are obtained for the source signals. DOA angle for each source is found as explained in the previous section and in equations (5)–(14).

[37] SNR is set as $SNR = 10\log_{10}\sigma_{s_1}{}^2$ where $\sigma_{s_1}{}^2$ is the average power of the first signal and the noise variance is $\sigma_n^2 = 1$. The threshold for the construction of binary image is half the maximum value of the STFT magnitude. STFT uses a Chebyshev window of length 48. The IF segments shorter than 20 pixels are deleted in the binary image. NSA algorithm is compared with the

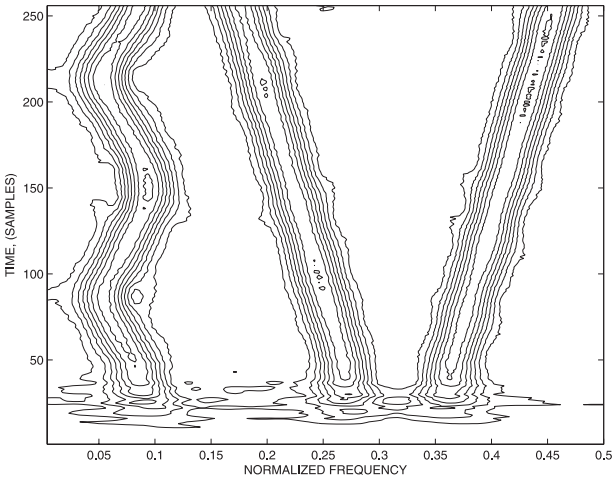

Figure 1. STFT distribution of the first sensor signal. *SNR* = 15 dB.

MUSIC and conventional (or benchmark) CRB. STFT-MUSIC represents the MUSIC algorithm with search process applied on the same data that the NSA algorithm uses where the source signals are isolated. Therefore sample covariance matrix of $\mathbf{S_x}(t_k, f_k)/S_{\mathbf{x}_k}(1)$ is constructed and used for a single source. CRB-PPS is the Cramer-Rao bound for the polynomial phase signals [*Gershman et al.*, 2001]. Figures 3–10, 13, and 15 show the Root Mean Square Error (RMSE) for the source DOA angles and therefore it reflects the average error in case of multiple sources.

[38] In Figure 3, different algorithms are compared when the number of sensors is $M = 3$. Figure 3a shows the performance of the algorithms for a single source at 70 degrees. NSA performs well and there is no flooring effect due to "cross talk" for the RMSE since there is only a single source. Figure 3b shows the performance comparison when there are two sources at 70 and 105 degrees. The flooring effect can be seen at high SNR. It is also observed that there is a significant difference between the observed performances and the CRB-PPS for the multiple sources. This is mainly due to the fact that none of the algorithms take advantage of the model for the polynomial phase signals. In our case, this allows us to deal with any kind of signal characteristics.

[39] Figure 4 shows the performance of the algorithms for a single source at 70 degrees when $M = 8$. Figures 3 and 4 show that NSA is close to the conventional CRB for single source scenario.

[40] Figure 5 shows the RMSE versus SNR performance when the source DOA angles are well separated, namely at 70, 90 and 105 degrees, respectively. NSA and STFT-MUSIC perform similarly and they are better than the conventional CRB even at low SNR. In Figure 6, the same experiment is repeated when the first two sources are at 95 degrees and the third source is at 115 degrees. Conventional CRB and MUSIC are not shown in Figure 6 since they fail in this experiment. The performance of the NSA and STFT-MUSIC is similar to the previous case in Figure 5 and they perform even when the sources have the same DOA. Figure 7 shows the performance when the number of snapshots, N, is changed. NSA performs well as long as $N \geq 40$ where the IF tracks for the sources are identified correctly. In Figure 8, $N = 256$ but we select only K time-frequency points for the computation of (5). Figure 8 shows the performance of the proposed algorithm when the K value is changed. A small number of time-frequency points are sufficient for a good performance which is an important advantage compared to the methods that use WVD. In case of WVD, cross terms can be suppressed only when K is significantly large [*Zhang and Amin*, 2000]. Figure 9 shows the performance when the two sources at 70 and 105 degrees are fixed and the third source is swept with one degree steps. NSA performs significantly better than the conventional CRB and has a uniform performance for all source angles. STFT-MUSIC and NSA have almost the same performance and they are plotted on top of each other. Figure 10 shows the performance of the proposed approach for the estimation of the elevation angle using equation (15). SNR is set to 15*dB* and the performance is outlined for different elevation angles for a single source at 70 degrees azimuth angle.

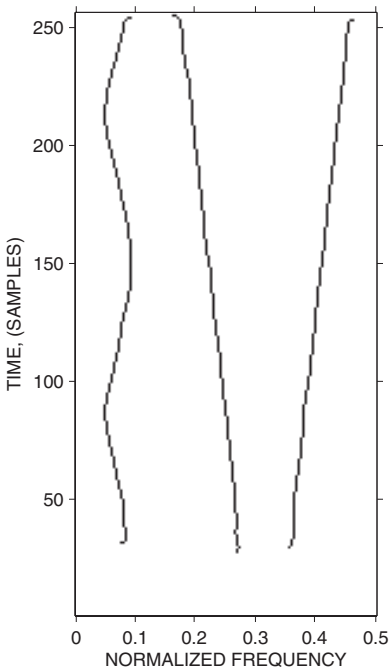

Figure 2. IF tracks for the source signals. *SNR* = 15 dB.

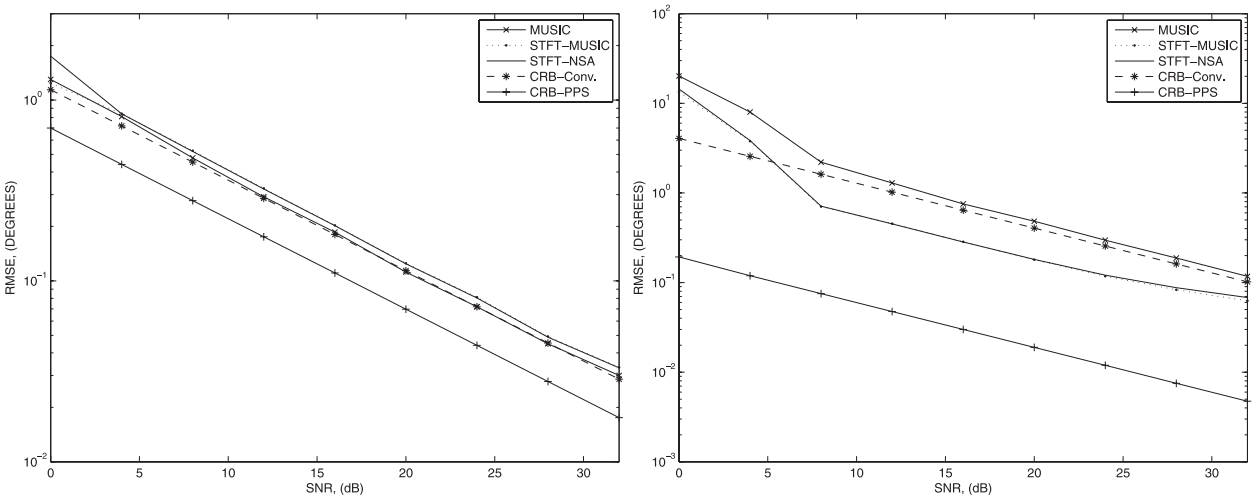

Figure 3. $M = 3$ and (a) single source at 70 degrees, (b) two sources at 70 and 105 degrees.

[41] The results of the above experiments show that the proposed approach has very good performance compared to the conventional methods. However the performance of the NSA algorithm does not get very close to the CRB-PPS due to the fact that we do not assume any signal model in time-frequency plane.

6.2. Overlapping Sources

[42] The simulation parameters are same as described above except the discrete-time chirp rates and center frequencies. The center frequencies are $w_{1,0} = \pi/5$, $w_{2,0} = 0$ and $w_{3,0} = \pi$, respectively. The discrete-time chirp rates in this case are set as $w_{1,1} = \pm 0.0032$, $w_{2,1} = -0.0063$ and $w_{3,1} = 0.0063$, respectively, for the source signals. In Figure 11a, the STFT of the three sources are shown for the $SNR = 10dB$. After the morphological image processing operations in section 4 are applied, the histogram of the DOA angles of the three sources are obtained as in Figure 12 at the fourth step of the proposed algorithm. When the CLEAN algorithm is used at the sixth step, isolated source in Figure 11b is obtained. Figure 11c

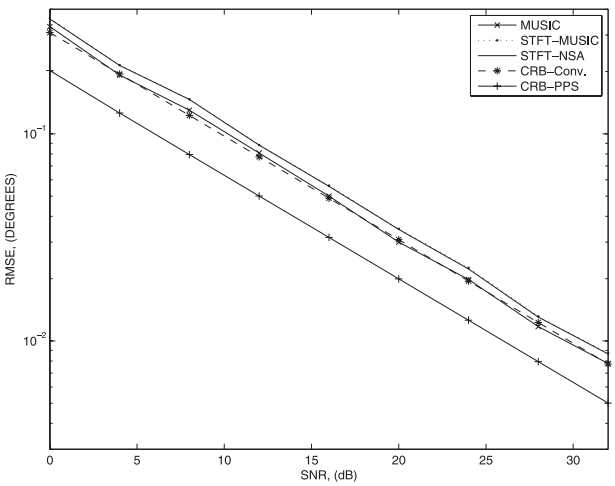

Figure 4. $M = 8$ and DOA performance for a single source at 70 degrees.

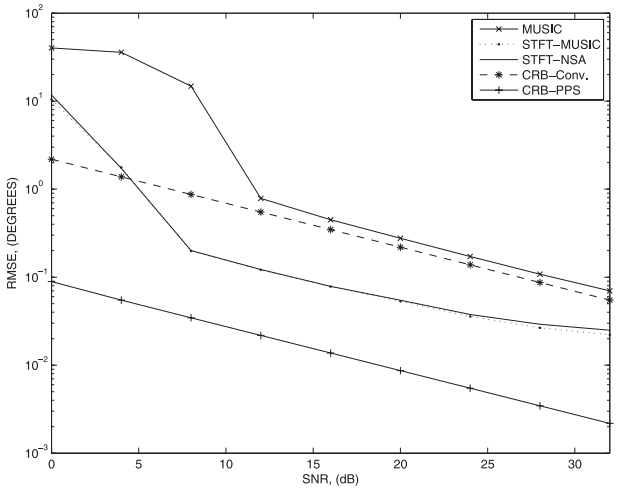

Figure 5. DOA performance for three sources at 70, 90, and 105 degrees.

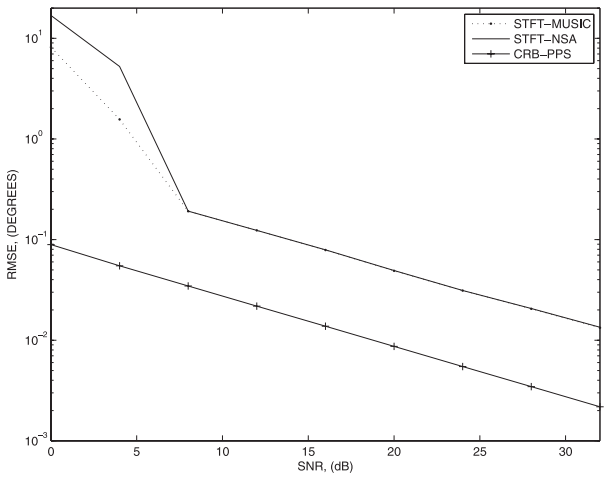

Figure 6. DOA performance for three sources at 95, 95, and 115 degrees.

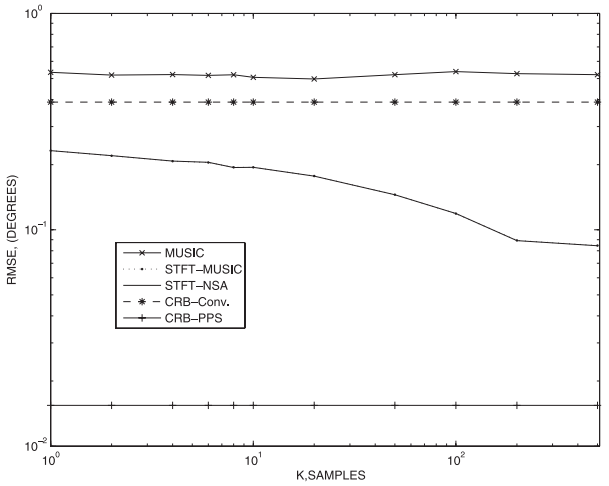

Figure 8. Performance in terms of the number of samples used for each IF track. *SNR* = 15 dB; DOA angles are 70, 90, and 105 degrees, respectively.

shows the binary image superimposed on the true IF track of the source. Figures 11d and 11e show the corresponding plots for the second and third sources. As it is seen from Figure 11, estimated IF tracks closely follow the true IF tracks. In Figure 13, the DOA estimation performance for the overlapping sources is shown. Proposed method performs better than the conventional techniques and it gives lower RMSE than the conventional CRB except at low SNR. At low SNR, STFT-MUSIC seems to perform better than STFT-NSA. A flooring effect is seen similar to the previous cases due to multiple sources. The performance for the overlapping sources is slightly worse than the case of nonoverlapping sources as can be seen from Figure 5. We also considered the case where the source powers are significantly different. In this case, the initial source amplitudes, c_k, are selected as, $c_1 = \sqrt{2}$, $c_2 = 1$ and $c_3 = 1/4$, respectively. Figure 14 shows the STFT magnitude for the three sources. As seen from Figure 14, the third source which is obvious in Figure 11, is hardly seen. The threshold for obtaining the binary image is set to 1/10

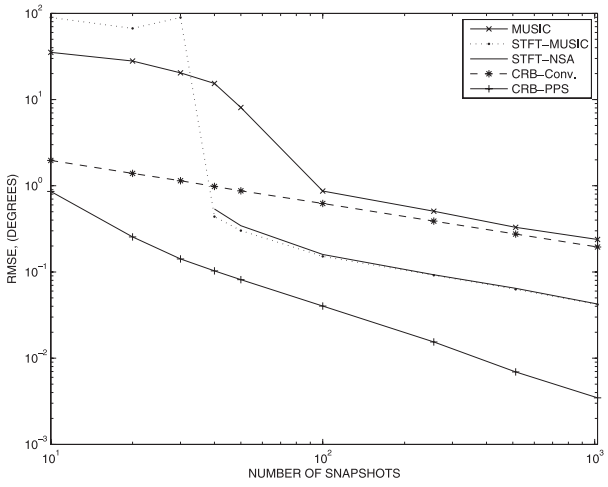

Figure 7. Performance in terms of the number of snapshots. *SNR* = 15 dB, DOA angles are 70, 90, and 105 degrees, respectively.

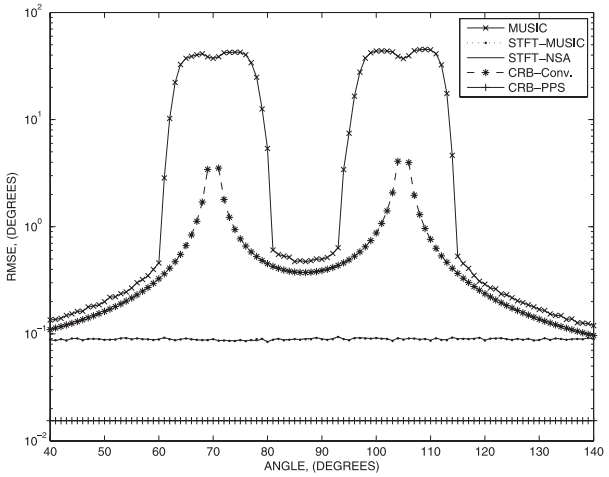

Figure 9. Two sources at 70 and 105 degrees are fixed, and the third source is swept. *SNR* = 15 dB.

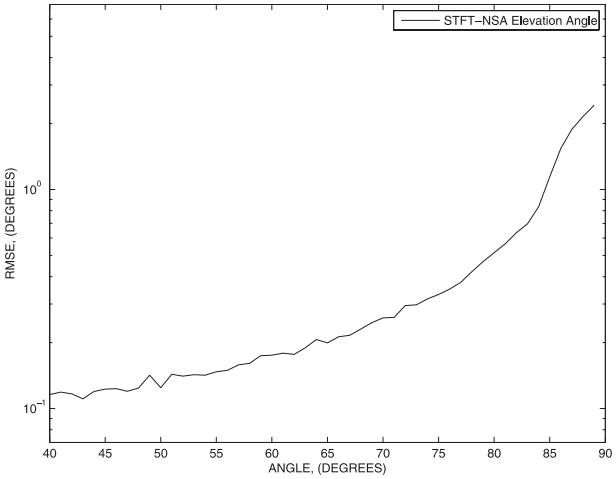

Figure 10. Elevation angle performance of the NSA. *SNR* = 15 dB.

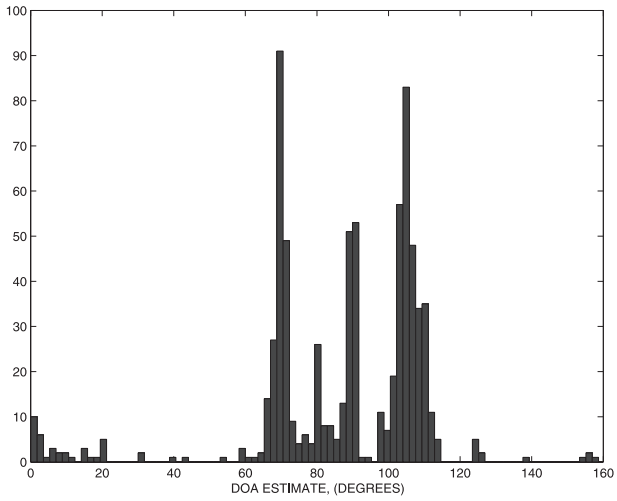

Figure 12. Histogram of the DOA estimates for the three overlapping sources at 70, 90, and 105 degrees, *SNR* = 10 dB.

of the maximum value. In this case, the computational complexity is increased due to the increase in the number of nonzero pixels at the fourth step of NSA. Figure 15 shows the DOA performance for each source separately. Although the third source has the lowest power, it is also effectively identified and accounted for by the proposed method. On the contrary, MUSIC algorithm fails since the DOA angle of the third source cannot be found accurately.

[43] The proposed method performs well in a variety of cases. It is usually better than the conventional CRB while it does not get very close to the CRB-PPS due to the fact that PPS model is not exploited and instead a more general approach is followed in order to deal with arbitrary signal characteristics. While a chirp beamformer [*Gershman et al.*, 2001] can be employed to solve the same problem, it has a bias which does not decrease with the increase of SNR. Furthermore it requires a multidimensional search over the parameter space. It is possible to define a polynomial-phase beamformer to process more general PPS but this increases the dimension of the search space. The proposed method does not have a significant bias as in chirp beamformer but it is affected by the finite sidelobe of the analysis window in STFT as well as the nonstationarity of the source signals. This introduces a flooring effect at high SNR for multiple sources. Overall, NSA is an effective

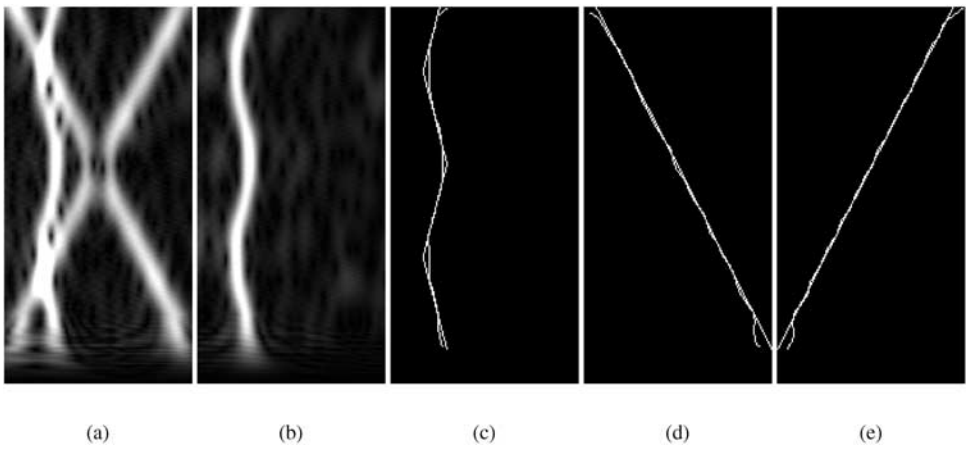

Figure 11. SNR = 10 dB and (a) STFT of the three sources, (b) STFT of the isolated first source, (c) IF of the first source, (d) IF of the second source, and (e) IF of the third source.

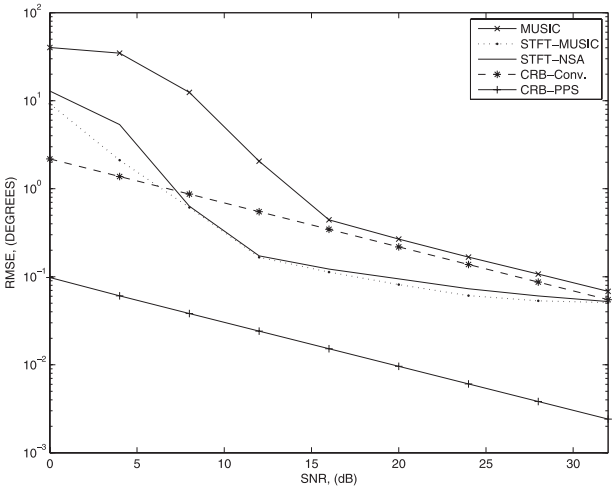

Figure 13. DOA performance of the three overlapping sources at 70, 90, and 105 degrees.

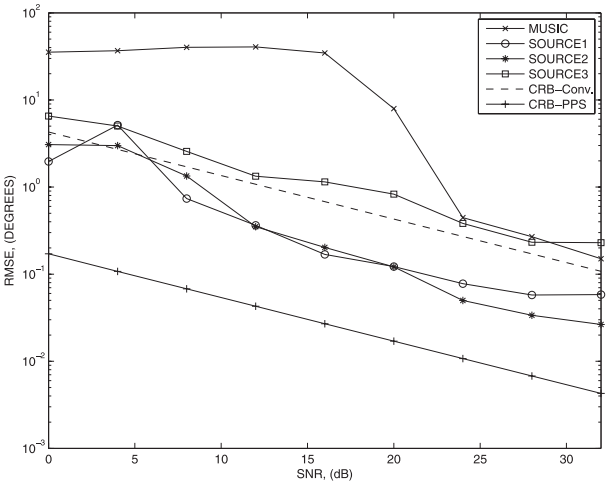

Figure 15. Performance for the three overlapping sources in Figure 14.

algorithm for DOA estimation in the time-frequency plane.

7. Conclusions

[44] A no-search algorithm is presented for DOA estimation. NSA eliminates the search required for arbitrary array geometries. The proposed method converts the multisource DOA estimation to a single source case by using morphological image processing in STFT distribution. Both overlapping and nonoverlapping sources are considered. IF tracks of the source signals are found automatically in each case and there is no assumption on the model of the source signals in time-frequency plane.

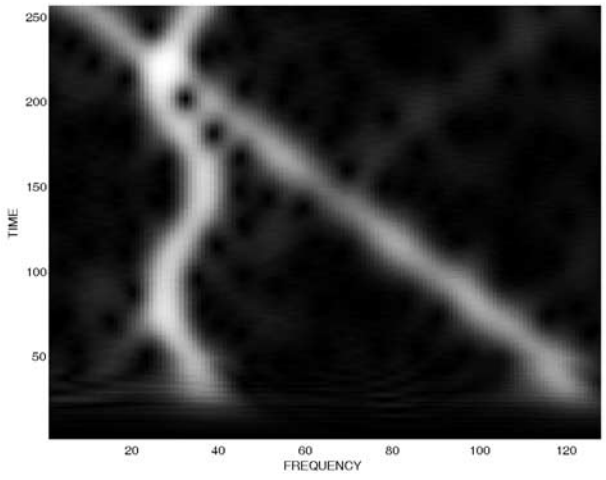

Figure 14. STFT distribution for the three sources at $SNR = 10$ dB.

The CLEAN algorithm is adopted in order to obtain the IF tracks of the sources. It is shown that the proposed method can effectively extract the IF tracks even when the source powers are different. While the proposed approach can be applied for arbitrary array geometries, UCA offers certain advantages. The properties of the UCA under this context are derived and it is shown that an indirect but least squares optimum solution of a linear matrix equation for DOA estimation performs better than the direct solution. Several simulations are done for the uniform circular array and it is shown that the performance of the NSA is between the conventional CRB and CRB for the polynomial phase signals. It performs significantly better than the conventional techniques in a variety of cases.

Appendix A

Proof of Lemma 1

$$\text{(a)} \qquad \sum_{j=1}^{M} dx_j = r \sum_{j=1}^{M} \cos\left(\frac{2\pi}{M}(j-1)\right) = 0 \qquad \text{(A1)}$$

$$\text{(b)} \qquad \sum_{j=1}^{M} dy_j = r \sum_{j=1}^{M} \sin\left(\frac{2\pi}{M}(j-1)\right) = 0 \qquad \text{(A2)}$$

$$\text{(c)} \qquad \sum_{j=1}^{M} dx_j dy_j = \frac{r^2}{2} \sum_{j=1}^{M} \sin\left(\frac{4\pi}{M}(j-1)\right) = 0 \qquad \text{(A3)}$$

(d) $$\sum_{j=2}^{M}\left(dx_j - dx_1\right)\left(dy_j - dy_1\right) = \sum_{j=2}^{M}\left(dx_i dy_i + dx_1 dy_1 - dx_1 dy_i - dx_i dy_1\right) = (M+1)dx_1 dy_1 = 0 \quad \text{(A4)}$$

since $dy_1 = 0$.

(e) $$\sum_{j=1}^{M} dx_j^2 = r^2 \sum_{j=1}^{M} \cos^2\left(\frac{2\pi}{M}(j-1)\right) = c_1 = \frac{r^2}{2}M \quad \text{(A5)}$$

(f) $$\sum_{j=1}^{M} dy_j^2 = r^2 \sum_{j=1}^{M} \sin^2\left(\frac{2\pi}{M}(j-1)\right) = r^2 \sum_{j=1}^{M}\left[1 - \cos^2\left(\frac{2\pi}{M}(j-1)\right)\right] = c_1 = \frac{r^2}{2}M \quad \text{(A6)}$$

The elements of the matrix $\mathrm{D}^H\mathrm{D}$ are

(g) $$\sum_{j=1}^{M} dx_j dy_j = \frac{r^2}{2}\sum_{j=1}^{M} \sin\left(\frac{4\pi}{M}(j-1)\right) = 0 \quad \text{(A7)}$$

$$\sum_{j=1}^{M} dx_j dz_j = z_0 \sum_{j=1}^{M} dx_j = 0 \quad \text{(A8)}$$

$$\sum_{j=1}^{M} dy_j dz_j = z_0 \sum_{j=1}^{M} dy_j = 0 \quad \text{(A9)}$$

and from e) and f), we have $\mathrm{D}^H\mathrm{D} = diag(c_1, c_1, Mz_0)$.

Proof of Theorem 1

We assume a planar uniform circular array with the z coordinate, $z_0 = 0$. If $z_0 \neq 0$, then it is always possible to define a new coordinate system with $z_0 = 0$. Therefore singular value decomposition of $M \times 2$ matrix D is,

$$\mathbf{D} = \mathbf{U}\begin{bmatrix}\sum \\ \mathbf{0}\end{bmatrix}\mathbf{V}^H \quad \text{(A10)}$$

where U and V are orthonormal matrices. Then we have,

$$\mathbf{D}\mathbf{D}^H = \mathbf{U}\begin{bmatrix}\sum^2 & \mathbf{0} \\ \mathbf{0} & \mathbf{0}\end{bmatrix}\mathbf{U}^H \quad \text{(A11)}$$

and

$$\mathbf{D}^H\mathbf{D} = \mathbf{V}\sum{}^2\mathbf{V}^H = c_1\mathbf{I} \quad \text{(A12)}$$

Owing to equation (A12), $\mathbf{\Sigma}^2 = c_1\mathrm{I}$ where c_1 is defined in Lemma 1. Since 2×2 matrix V is orthonormal, $\mathrm{V}\mathrm{V}^H = \mathrm{V}^H\mathrm{V} = \mathrm{I}$. Therefore V is either identity, V = I, or it is a permutation matrix of,

$$\mathbf{V} = \begin{bmatrix}0 & 1 \\ 1 & 0\end{bmatrix} \quad \text{(A13)}$$

We assume that V = I for simplicity. Otherwise the same steps can be easily followed for the case of the permutation matrix, which changes the order of the vectors in consideration, to complete the proof. Considering equation (A10), $\mathrm{D} = [\mathrm{u}_1\ \mathrm{u}_2\ \ldots\ \mathrm{u}_M]$ and $\mathbf{\Sigma} = diag(\sqrt{c_1}, \sqrt{c_1})$. Therefore

$$\mathbf{D} = [\sqrt{c_1}\mathbf{u}_1 \quad \sqrt{c_1}\mathbf{u}_2] \quad \text{(A14)}$$

Then the Moore-Penrose pseudoinverse,

$$\overline{\mathbf{G}} = \left(\mathbf{D}^H\mathbf{D}\right)^{-1}\mathbf{D}^H = (1/\sqrt{c_1})\begin{bmatrix}\mathbf{u}_1^H \\ \mathbf{u}_2^H\end{bmatrix} \quad \text{(A15)}$$

The Wiener matrix in Theorem 1 is $\mathbf{G} = \sigma_\psi^2\mathbf{D}^H(\sigma_\psi^2\mathbf{D}\mathbf{D}^H + \sigma_e^2\mathbf{I})^{-1}$. $\sigma_\psi^2\mathbf{D}\mathbf{D}^H + \sigma_e^2\mathbf{I}$ has the same eigenvectors of $\mathbf{D}\mathbf{D}^H$. Therefore, $(\sigma_\psi^2\mathbf{D}\mathbf{D}^H + \sigma_e^2\mathbf{I})^{-1} = \mathbf{U}\mathbf{\Lambda}\mathbf{U}^{\mathrm{H}}$ where $\mathbf{\Lambda} = diag((\sigma_\psi^2 c_1 + \sigma_e^2)^{-1}\ (\sigma_\psi^2 c_1 + \sigma_e^2)^{-1}\ (\sigma_e^2)^{-1}\ \ldots\ (\sigma_e^2)^{-1})$. Then using equations (A11) and (A14), we have

$$\mathbf{G} = \sigma_\psi^2\mathbf{D}^H\left(\sigma_\psi^2\mathbf{D}\mathbf{D}^H + \sigma_e^2\mathbf{I}\right)^{-1} = \frac{\sigma_\psi^2\sqrt{c_1}}{\sigma_\psi^2 c_1 + \sigma_e^2}\begin{bmatrix}\mathbf{u}_1^H \\ \mathbf{u}_2^H\end{bmatrix} \quad \text{(A16)}$$

Therefore we have $\mathbf{G} = \frac{\sigma_\psi^2 c_1}{\sigma_\psi^2 c_1 + \sigma_e^2}\overline{\mathbf{G}}$.

[45] **Acknowledgment.** This work is supported by the Turkish Scientific and Technological Research Council by the project 104E045.

References

Abramovich, Y. I. (1978), A recursive method for the resolution of wideband signals with substantially different intensities, *Radio Eng. Electron. Phys.*, *23*(8), 66–70.

Aissa-El-Bey, A., N. Linh-Trung, K. Abed-Meraim, A. Belouchrani, and Y. Grenier (2007), Underdetermined blind separation of nondisjoint sources in the time-frequency domain, *IEEE Trans. Signal Process.*, *55*(3), 897–907.

Barkat, B., B. Boashash, and L. J. Stankovic (1999), Adaptive window in the PWVD for the IF estimation of FM signals in additive Gaussian noise, in *Proceedings of International Conference on Acoustics, Speech, and Signal Processing, ICASSP-1999*, vol. 3, pp. 1317–1320, IEEE Press, Piscataway, N. J.

Belouchrani, A., and M. G. Amin (1999), Time-frequency MUSIC, *IEEE Signal Process. Lett.*, *6*(5), 109–110.

Borda, M., I. Nafornita, D. Isar, and A. Isar (2005), New instantaneous frequency estimation method based on image processing techniques, *J. Electron. Imaging*, *14*(2).

Clark, B. G. (1980), An efficient implementation of the algorithm 'CLEAN', *Astron. Astrophys.*, *89*, 377–378.

Davydenko, M. A., N. V. Ilyin, and V. V. Khakhinov (2008), A method for restoration of radio channel transfer function by chirp sounding of the ionosphere, *Int. J. Geomagn. Aeron.*, *7*, GI3006, doi:10.1029/2006GI000158.

Deng, H. (2004), Effective CLEAN algorithms for performance-enhanced detection of binary coding radar signals, *IEEE Trans. Signal Process.*, *52*(1), 72–78.

Dougherty, E. R., and R. A. Lotufo (2003), *Hands-on Morphological Image Processing*, vol. TT59, SPIE, Bellingham, Wash.

Gershman, A. B., and M. G. Amin (2000), Wideband direction of arrival estimation of multiple chirp signals using spatial time-frequency distributions, *IEEE Signal Process. Lett.*, *7*(6), 152–155.

Gershman, A. B., M. Pesavento, and M. G. Amin (2001), Estimating parameters of multiple wideband polynomial-phase sources in sensor arrays, *IEEE Trans. Signal Process.*, *49*(12), 2924–2933.

Heidenreich, P., L. A. Cirillo, and A. M. Zoubir (2007), Direction finding of nonstationary signals using spatial time-frequency distributions and morphological image processing, in *Proceedings of International Conference on Acoustics, Speech, and Signal Processing, ICASSP-2007*, vol. 3, pp. 1137–1140, IEEE Press, Piscataway, N. J.

Hirari, M., and M. Hayakawa (1999), Direction of arrival estimation using blind separation of sources, *Radio Sci.*, *34*(3), 693–701.

Högbom, J. (1974), Aperture synthesis with a non-regular distribution of interferometer baselines, *Astron. Astrophys.*, *15*, 417–426.

Parkinson, M. L., P. L. Dyson, and P. R. Smith (1997), Analysis of direction of arrival aliasing for MF/HF Doppler-sorted interferometry measurements of ionospheric drift, *Radio Sci.*, *32*(3), 999–1009.

Schwarz, U. J. (1978), Mathematical-statistical description of the iterative beam removing technique (Method CLEAN), *Astron. Astrophys.*, *65*, 345–356.

Stankovic, L. J., S. Stankovic, and I. Djurovic (1997), An architecture for realization of the cross-terms free polynomial Wigner-Ville distribution, in *Proceedings of International Conference on Acoustics, Speech, and Signal Processing, ICASSP-1997*, vol. 3, pp. 2053–2056, IEEE Press, Piscataway, N. J.

Stoica, P., and R. Moses (2005), *Spectral Analysis of Signals*, Prentice-Hall, Upper Saddle River, N. J.

Stoica, P., and A. Nehorai (1990), MUSIC, maximum likelihood, and Cramer-Rao bound: further results and comparisons, *IEEE Trans. Signal Process.*, *38*(12), 2140–2150.

Tsao, J., and B. D. Steinberg (1988), Reduction of sidelobe and speckle artifacts in microwave imaging: The CLEAN Technique, *IEEE Trans. Antennas Propag.*, *36*(4), 543–556.

Tuncer, T. E., and B. Friedlander (2009), *Classical and Modern Direction-of-Arrival Estimation*, Academic, San Diego, Calif.

Tuncer, T. E., T. K. Yasar, and B. Friedlander (2007), Direction of arrival estimation for nonuniform linear arrays by using array interpolation, *Radio Sci.*, *42*, RS4002, doi:10.1029/2007RS003641.

Weiss, A. J., and B. Friedlander (1993), On the Cramer-Rao bound for direction finding of correlated signals, *IEEE Trans. Signal Process.*, *41*(1), 495–499.

Weiss, A. J., and B. Friedlander (1996), Array processing using joint diagonalization, *Signal Process.*, *50*, 205–222.

Zhang, Y., and M. G. Amin (2000), Spatial averaging of time-frequency distributions for signal recovery in uniform linear arrays, *IEEE Trans. Signal Process.*, *48*(10), 2892–2902.

Zhou, H., B. Wen, S. Wu, and X. Liu (2004), Linear time-frequency MUSIC algorithm, in *Proceedings of 6th CAS Symposium on Emerging Technologies: Mobile and Wireless Communications, Shanghai, China, May 31 to June 2*, IEEE Press, Piscataway, N. J.

M. T. Özgen, Electrical and Electronics Engineering Department, Anadolu University, 26470 Eskişehir, Turkey. (mtozgen@anadolu.edu.tr)

T. E. Tuncer, Electrical and Electronics Engineering Department, Middle East Technical University, 06531Ankara, Turkey. (etuncer@metu.edu.tr)